CHIN. PHYS. LETT. Vol. 37, No. 5 (2020) 057301

Electrically Tunable Wafer-Sized Three-Dimensional Topological Insulator Thin Films Grown by Magnetron Sputtering *

Qixun Guo(郭奇勋)[1], Yu Wu(吴宇)[1], Longxiang Xu(徐龙翔)[1], Yan Gong(龚演)[2], Yunbo Ou(欧云波)[2], Yang Liu(刘洋)[1], Leilei Li(李磊磊)[1], Yu Yan(岩雨)[3**], Gang Han(韩刚)[4], Dongwei Wang(王东伟)[5], Lihua Wang(王立华)[6], Shibing Long(龙世兵)[7], Bowei Zhang(张博威)[8], Xun Cao(曹迅)[8], Shanwu Yang(杨善武)[4], Xuemin Wang(王学敏)[4], Yizhong Huang(黄一中)[8], Tao Liu(刘涛)[9], Guanghua Yu(于广华)[1], Ke He(何珂)[2**], Jiao Teng(滕蛟)[1**]

[1]*Department of Material Physics and Chemistry, University of Science and Technology Beijing, Beijing 100083*
[2]*State Key Laboratory of Low-Dimensional Quantum Physics, Tsinghua University, Beijing 100084*
[3]*Corrosion and Protection Center, Key Laboratory for Environmental Fracture (MOE), Institute of Advanced Materials and Technology, University of Science and Technology Beijing, Beijing 100083*
[4]*Collaborative Innovation Center of Advanced Steel Technology, University of Science and Technology Beijing, Beijing 100083*
[5]*CAS Key Laboratory of Standardization and Measurement for Nanotechnology, National Center for Nanoscience and Technology, Beijing 100190*
[6]*Institute of Microstructure and Property of Advanced Materials, Beijing Key Lab of Microstructure and Property of Advanced Materials, Beijing University of Technology, Beijing 100124*
[7]*School of Microelectronics, University of Science and Technology of China, Hefei 230026*
[8]*School of Materials Science and Engineering, Nanyang Technological University, 50 Nanyang Avenue, 639798, Singapore*
[9]*Department of Physics, The Ohio State University, Columbus, Ohio 43210, USA*

(Received 2 March 2020)

Three-dimensional (3D) topological insulators (TIs) are candidate materials for various electronic and spintronic devices due to their strong spin-orbit coupling and unique surface electronic structure. Rapid, low-cost preparation of large-area TI thin films compatible with conventional semiconductor technology is the key to the practical applications of TIs. Here we show that wafer-sized Bi_2Te_3 family TI and magnetic TI films with decent quality and well-controlled composition and properties can be prepared on amorphous SiO_2/Si substrates by magnetron cosputtering. The SiO_2/Si substrates enable us to electrically tune $(Bi_{1-x}Sb_x)_2Te_3$ and Cr-doped $(Bi_{1-x}Sb_x)_2Te_3$ TI films between p-type and n-type behavior and thus study the phenomena associated with topological surface states, such as the quantum anomalous Hall effect (QAHE). This work significantly facilitates the fabrication of TI-based devices for electronic and spintronic applications.

PACS: 73.50.−h, 75.50.Pp, 75.70.−i DOI: 10.1088/0256-307X/37/5/057301

Three-dimensional (3D) topological insulators (TIs) have a bulk gap and gapless surface states including an odd number of Dirac cones in a surface Brillouin zone.[1,2] The topological surface states are spin-momentum-locked and are protected by time-reversal symmetry from perturbations such as structural defects, disorder and nonmagnetic impurities. Various exotic quantum effects have been observed or predicted in TI-based materials or structures, such as the quantum anomalous Hall effect (QAHE), topological magnetoelectric effect and chiral Majorana fermions. These effects can be used to develop low-energy-consumption electronic devices and topological quantum computers. Recently, TIs have also attracted much attention for their possible applications in spintronic devices.[3−12]

Integrating TIs into the mature semiconductor technology is of key importance to realize their full potential for electronic or spintronic applications. Currently, 3D TI materials are mainly prepared by bulk Bridgman growth,[13−15] chemical vapor deposition (CVD)[16,17] or molecular beam epitaxy (MBE).[18−20] It is difficult to obtain large-area 3D TI films with well-controlled properties by Bridgman growth, and CVD-grown TI films usually need to be transferred from the growth substrate onto other substrates for various electronic devices. On the other hand, the low growth rate and high cost (especially for large wafers) of MBE make it less favored for the mass production of TI-based materials and devices. Magnetron sputtering is a low-cost, high-yield growth method compatible with conventional semiconductor technology. The method is particularly capable of fabricating thin films with complex structures and compositions, which is crucial for applications of TI materials in various devices. However, samples grown by magnetron sputtering are

*Supported by the National Key R&D Plan Program of China (Grant No. 2017YFF0206104), the National Key Scientific Research Projects of China (Grant No. 2015CB921502), the National Natural Science Foundation of China (Grant Nos. 61574169 and 51871018), Beijing Laboratory of Metallic Materials and Processing for Modern Transportation, the Opening Project of Key Laboratory of Microelectronics Devices & Integrated Technology, Institute of Microelectronics of Chinese Academy of Sciences, Beijing Natural Science Foundation (Grant No. Z180014), and Beijing Outstanding Young Scientists Projects (Grant No. BJJWZYJH01201910005018).
**Corresponding author. Email: yanyu@ustb.edu.cn; kehe@tsinghua.edu.cn; tengjiao@mater.ustb.edu.cn
© 2020 Chinese Physical Society and IOP Publishing Ltd

polycrystalline and usually have rather low carrier mobility, which restricts the applications of this technique to the growth of semiconductor materials.[21,22]

In this study, we grew wafer-sized Bi_2Te_3 family TI films on usual amorphous SiO_2/Si substrates through magnetron sputtering and found that due to the layered structure of the materials, the films have decent quality with a carrier mobility up to 310 cm^2/Vs, comparable to that of the films grown with MBE. Topological surface states were observed in the samples with angle-resolved photoemission spectroscopy (ARPES). The SiO_2/Si substrates enable us to gate-tune the carrier density of TI films grown on them, and in $(Bi,Sb)_2Te_3$ films with an appropriate Bi/Sb ratio, the ambipolar field effect is realized. With magnetron sputtering, we also realized the growth of magnetically doped TI $Cr_y(Bi_xSb_{1-x})_{2-y}Te_3$ (CBST) films that show ferromagnetism with an out-of-plane easy magnetization axis. An anomalous Hall resistance (R_{AH}) up to 16.4 kΩ was observed at 2 K, promising the observation of the QAHE in the films. These results demonstrate magnetron sputtering as a suitable mass production method for growing TI-based films for various electronic and spintronic applications.

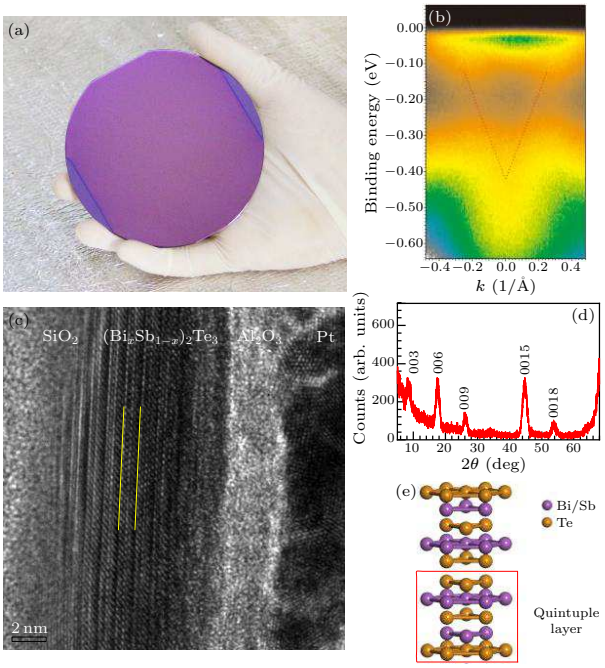

Fig. 1. Structural characterization of Bi_2Te_3 and BST thin films grown on amorphous SiO_2/Si by magnetron sputtering. (a) Photograph of a Bi_2Te_3/SiO_2 film with a diameter of 10 cm. (b) Electronic band structure of a Bi_2Te_3 thin film measured by ARPES showing linear dispersion of topological surface states (red dashed line). (c) HRTEM image and (d) XRD pattern of a BST thin film grown on amorphous SiO_2 (sample BST2). (e) The rhombohedral crystal structures of Bi_2Te_3 and $(Bi_{1-x}Sb_x)_2Te_3$.

We grew $(Bi_{1-x}Sb_x)_2Te_3$ films by cosputtering Bi_2Te_3 and Sb_2Te_3 alloy targets as well as Te targets on amorphous SiO_2/Si(100) substrates, which were kept at 160 ℃ during growth. By modifying the Bi/Sb ratio in the films, one can control the density as well as the type of carriers in the films. The Bi/Sb ratio in the films was controlled by the sputtering powers of the Bi_2Te_3 and Sb_2Te_3 target guns. The Te target was also turned on at the same time to reduce the Te deficiency in the films. After growth, the films were annealed at 160 ℃ for 25 min. Figure 1(a) shows a photograph of a 10 cm (4 inch) diameter silicon wafer with a 10 nm thick Bi_2Te_3 film grown on it, which maintains uniform properties across the whole film. Figure 1(c) displays a high-resolution transmission electron microscopy (HRTEM) cross-sectional image of a $(Bi_{1-x}Sb_x)_2Te_3$ film, which shows the characteristic quintuple-layer structure of Bi_2Te_3. Although the film is polycrystalline, all the grains have the same c orientation (normal to the cleavage plane). The crystalline structure of the BST film was further confirmed by x-ray diffraction (XRD) measurements (Fig. 1(d)). The presence of only $(0,0,3n)$ diffraction peaks suggests that the film plane is parallel to the cleavage plane. This postulation is reasonable because the material has a layered structure, which means that the cleavage surface has a quite low surface free energy. The above structural characterization results demonstrate that we can indeed obtain Bi_2Te_3 family TI films with decent crystalline quality via magnetron sputtering.

We used ARPES to assess the electronic band structure of a 10 QL-thick Bi_2Te_3 film grown by magnetron sputtering. Although the film is composed of domains of various in-plane crystalline orientations, the different domains have similar surface state band dispersion near the Dirac point because of the isotropy of the topological surface states around here, which will give observable ARPES signals. We indeed identified energy bands with similar band dispersion to the topological surface states of Bi_2Te_3 (Fig. 1(b)). The observation further confirms that we obtained Bi_2Te_3 TI films with magnetron sputtering, although the randomly orientated grains can significantly broaden the spectra.

For transport studies, we prepared three $(Bi_{1-x}Sb_x)_2Te_3$ samples, BST1, BST2 and BST3, with x = 0.74, 0.72 and 0.58, respectively. Figure 2(b) shows the R_{xx}–T curve of the BST2 film. At high temperatures (in the region of ∼88–300 K), R_{xx} increases with increasing T, showing semiconductor-like behavior and indicating that E_F is in the bulk band gap. The R_{xx}–T curve displays metallic behavior in the intermediate temperature region (∼7–88 K), which can be the result of reduced electron-phonon scattering of the surface states.[15,23,24] A second increase in R_{xx} when T is lower than 7 K can be ascribed to the electron-electron interaction to conduction, which is similar to those of the MBE-grown films of similar composition and thickness.[23–25]

Moreover, Fig. 2(c) shows the Hall resistance of sample BST2 as a function of magnetic field $R_{xy}(\mu_0 H)$ at various gate voltages. The R_{xy}–$\mu_0 H$ curves are always linear over the entire range of the magnetic field (±2 T), and the positive slopes of R_{xy}–$\mu_0 H$ as the

gate voltage V_g increases from -120 V to -15 V suggest that the dominant carriers are p-type, while the negative slopes of R_{xy}–$\mu_0 H$ as V_g continue to increase show that the dominant carriers are n-type. The zero-field longitudinal resistance R_{xx} and Hall coefficient R_H extracted from R_{xy}–$\mu_0 H$ curves of sample BST1-3 are plotted in Figs. 2(d)–2(f) as a function of gate voltage. In the case of BST1 (BST3), the R_{xx} monotonically increases (decreases) with increasing V_g, and the R_H has positive (negative) signs, indicating that BST1 (BST3) is a p-type (n-type) semiconductor. On the other hand, in sample BST2, when V_g is approximately 0 V, R_H reverses its sign, while R_{xx} reaches its maximum value. These results clearly demonstrate the ambipolar field effect of Dirac dispersions and suggest that the Fermi level can be controlled across the DP by tuning the ratio of Bi to Sb (Fig. 2(a)) and back-gate voltages. We note that for sample BST2, the maximum value of R_{xx}, corresponding to the gate voltage at the charge neutral point, is on the same order as the maximum values of BST samples deposited by CVD or MBE, as listed in Table 1, and is also in the same order as the quantum resistance. The 2D carrier densities $n_{2D} = 1/(eR_H)$ (where e is the elementary charge) can be obtained from the linear ordinary Hall resistance, and the lowest carrier density is $n_{2D} = 2.7 \times 10^{12}\,\mathrm{cm}^{-2}$ at $V_g = 60$ V with a corresponding mobility of $270\,\mathrm{cm}^2/\mathrm{Vs}$ for electrons, while the lowest carrier density is $n_{2D} = 2.3 \times 10^{12}\,\mathrm{cm}^{-2}$ at $V_g = -120$ V with a corresponding mobility of $310\,\mathrm{cm}^2/\mathrm{Vs}$ for holes. It can be concluded that magnetron sputtering is an effective method to prepare BST thin films with insulating bulk and low carrier densities, while the highly tunable Fermi level on SiO_2 allows us to explore the novel properties of topological surface states near the DP.

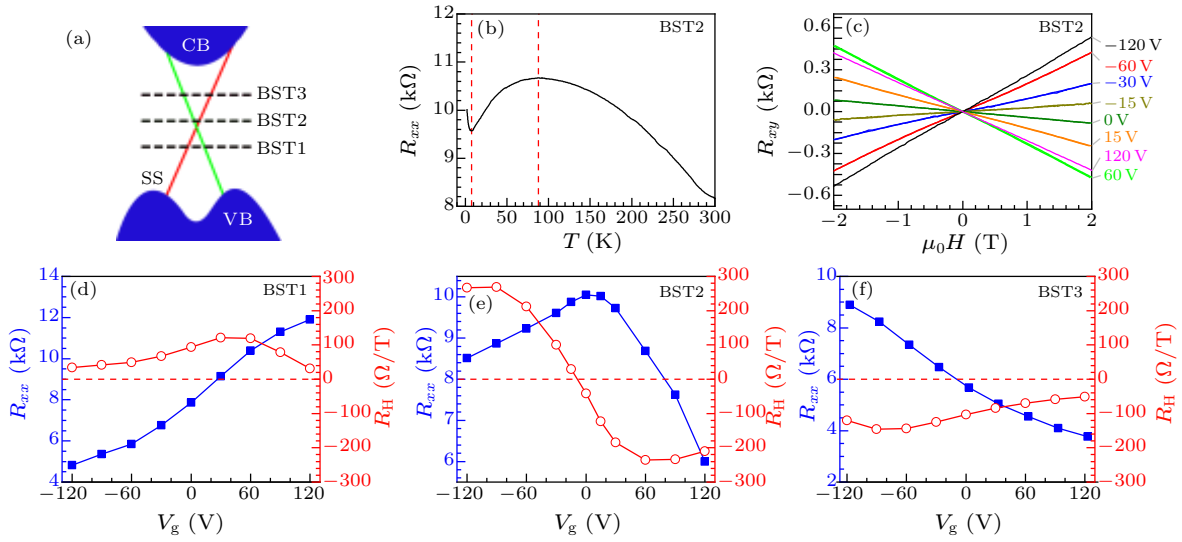

Fig. 2. Electrical transport in 7 nm thick BST thin films. (a) Schematic band structure for samples BST1, BST2 and BST3 and the corresponding Fermi levels, where CB, VB and SS are the bulk conduction band, bulk valance band and surface state, respectively. (b) The temperature (T) dependence of the longitudinal sheet resistance (R_{xx}) at zero magnetic field. From left to right, two red dashed lines are located at $T = 7$ K and $T = 88$ K, respectively. (c) Hall resistance R_{xy} as a function of magnetic field $\mu_0 H$ at 2 K tuned by the back-gate voltage. (d)–(f) Dependence of zero field longitudinal sheet resistance $R_{xx}(0)$ (solid squares) and Hall coefficient R_H (open circles) on the back-gate voltage for samples BST1 (d), BST2 (e) and BST3 (f) at $T = 2$ K.

Table 1. Gate-tuned longitudinal sheet resistance of BST samples developed by different techniques.

Device	R_{xx} (kΩ)	T (K)	Thickness	
CVD-grown BST	0.5–5.5	2	5 nm	Ref. [26]
MBE-grown BST	8–12	2.2	20 nm	Ref. [27]
	3–12	0.04	8 nm	Ref. [28]
	2–6	2.1	7 nm	Ref. [29]
	2–8	1.6	8 nm	Ref. [29]
	1–3	1.6	20 nm	Ref. [24]
	2–12	1.4	10 nm	Ref. [30]
	3–12	6.9	10 nm	Ref. [31]
Sputter-deposited BST	6–10	2	7 nm	This work

After the BST thin films with bulk insulating properties were successfully prepared, we focused on the Cr-doped TI thin films grown by magnetron sputtering to investigate the possibility of realizing long-range ferromagnetic order and tuning E_F inside the surface gap. One way to generate long-range ferromagnetic order in TIs is magnetic doping, and magnetically doped TI materials have been grown by CVD,[32] bulk Bridgman growth[33–36] and MBE.[37] Until now, however, magnetron sputtering has rarely been adopted for this purpose. In our experiment, CBST films were prepared by the cosputtering of Sb_2Te_3, Bi_2Te_3, Te and Cr targets at a substrate temperature of 175 ℃. Figure 3 presents an example of ferromagnetic properties observed in a 6 nm thick $Cr_{0.24}(Bi_{0.36}Sb_{0.64})_{1.76}Te_3$ film. At $T = 2$ K, the conventional butterfly-shaped $R_{xx} - \mu_0 H$ curve and nearly square-shaped Hall hysteresis loop with a coercive field of 340 Oe shown in Figs. 3(a) and 3(b) suggest that the long-range ferromagnetic order with perpendicular magnetic anisotropy is developed at low temperatures. A Curie temperature (T_c) of 11 K is de-

termined by an Arrott plot (Fig. 3(c)), in which R_{xy}^2 is plotted against $\mu_0 H/R_{xy}$ and the extrapolated intercept is proportional to the saturation magnetization.

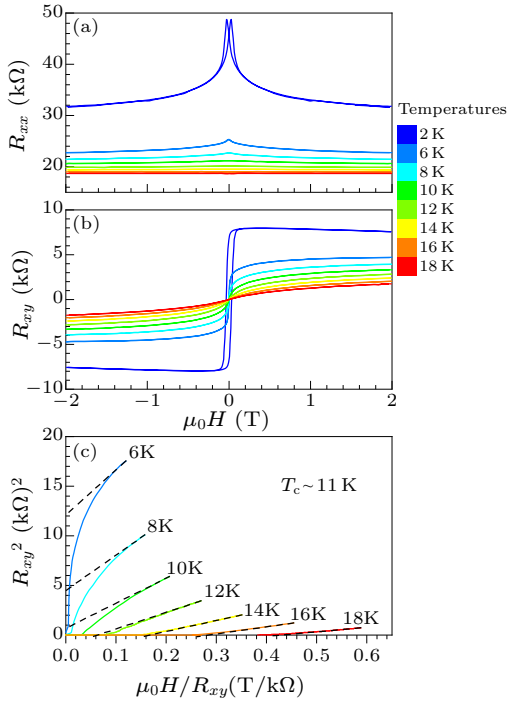

Fig. 3. Ferromagnetic characterization of a 6 nm thick CBST thin film. (a) Longitudinal resistance R_{xx} and (b) Hall resistance R_{xy} vs $\mu_0 H$ at different temperatures. (c) Arrott plot of the CBST thin film.

Generally, the Hall resistance of the anomalous Hall effect is expressed as[37,38]

$$R_{xy} = R_0 H + R_{\rm AH}(M), \tag{1}$$

where R_0 is the slope of the ordinary Hall background, H is the applied magnetic field, and M is the magnetization component in the perpendicular direction. Figures 4(a) and 4(b) present the longitudinal sheet resistance R_{xx} and Hall resistance R_{xy}, respectively, as a function of H of a CBST thin film at various back-gate voltages. $R_{\rm AH}$ estimated by the intercept of the linear background at a high magnetic field and zero field $R_{xx}(0)$ are plotted in Fig. 4(c). We observe that the $R_{\rm AH}$ and $R_{xx}(0)$ data point towards the same trend and both reach their maxima at $V_{\rm g} = -130$ V and their minima at $V_{\rm g} = 150$ V. It is worth noting that the maximum of $R_{\rm AH}$ in Fig. 4(c) is 16.4 kΩ, which exceeds 60% of the quantum Hall resistance (h/e^2). More importantly, the existence of robust ferromagnetic order in both p-type and n-type Cr-doped TI thin films grown by magnetron sputtering and the $V_{\rm g}$-independent coercive field shown in Fig. 4(b) demonstrate the occurrence of carrier-independent bulk van Vleck magnetism, which is consistent with the results reported in the literature.[37,39]

Nevertheless, the QAHE has not been observed in our Cr-doped TI films grown by magnetron sputtering. In the quantum anomalous Hall regime, $R_{\rm AH}$

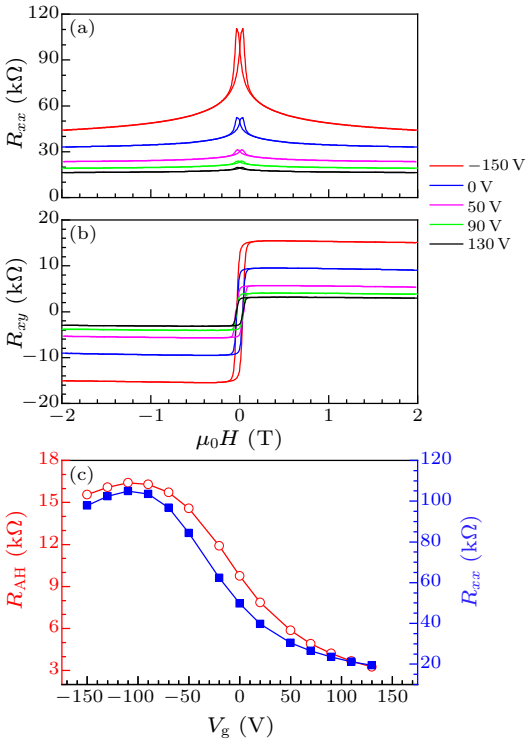

Fig. 4. (a) Longitudinal sheet resistance R_{xx} and (b) Hall resistance R_{xy} vs $\mu_0 H$ at different gate voltages at a temperature of 2 K. (c) $V_{\rm g}$-dependent $R_{\rm AH}$ (open circles) and $R_{xx}(0)$ (solid squares) measured at 2 K.

should reach a maximum, and R_{xx} should exhibit a dip at the charge neutral point.[20,40,41] This signature has not been observed in our CBST thin films at $T = 2$ K. The $R_{\rm AH}/R_{xx}(0)$ ratio of the CBST thin film, however, has a maximum of approximately 0.2 at $V_{\rm g} = 20$ V (see Fig. S6 in the Supplementary Materials), which exceeds the Hall angle of usual diluted magnetic semiconductors.[37] Therefore, the quantum anomalous edge states in CBST may contribute to carrier transport. We believe that it will be possible to observe the QAHE at 2 K or lower temperature in CBST thin films grown by magnetron sputtering if the quality of the sample is improved further by reducing the sputtering rate, controlling the amount of Cr more precisely and adjusting the annealing process, among other measures.

In summary, we have demonstrated that it is possible to grow Bi_2Te_3 family TI thin films on amorphous SiO_2/Si substrates by magnetron sputtering. Our work provides a large-scale method to produce bulk insulating TI thin films with tunable transport properties. Both the ARPES data and the ambipolar field effect point to the conclusion that the topological surface states can very well exist in these sputtered polycrystalline thin films. An unusually large value of 60% of the quantum anomalous Hall resistance is observed in Cr-doped BST films, and more efforts are needed to obtain an ideal quantum anomalous Hall insulator. The magnetron cosputtering growth provides a first yet important step towards the large-scale fabrication of multilayer films with complex structures for future spintronic devices.

Magnetron sputtering growth.—Bi_2Te_3, BST and CBST thin films were grown on polished, thermally oxidized silicon substrates (300 nm SiO_2/silicon) by magnetron sputtering. The cosputtering method with a high-purity (99.99%) Bi_2Te_3 alloying target, Sb_2Te_3 alloying target and Te target was adopted to control the films' composition. The BST thin films were deposited from Bi_2Te_3 and Sb_2Te_3 targets by dc sputtering and from a Te target by rf sputtering. The CBST thin films were deposited from Bi_2Te_3, Sb_2Te_3 and Cr (99.95%) targets by dc sputtering and a Te target by rf sputtering. During growth, the Si(100) substrate was kept at 160 ℃ for BST thin films and at 175 ℃ for CBST thin films. The base pressure of the deposition chamber was below 3×10^{-7} Torr, and the working argon pressure was set at 2×10^{-3} Torr. After growth, the thin films were annealed for 25 min at the same temperature as the deposition. When the substrate temperature was cooled to room temperature, a 3–4 nm thick Al thin film was sputtered *in situ* on the topological insulator thin films, and the Al thin film was naturally oxidized to form Al_2O_3 after the sample was removed from the chamber and exposed in air.

Material characterization.—To avoid possible contamination of Bi_2Te_3 thin films, a 2 nm thick Te capping layer was deposited on top of the films before we removed them from the high-vacuum growth chamber. The Bi_2Te_3 thin films with a 2 nm Te capping layer were exposed in air for two hours before ARPES measurements. ARPES data were collected by a Scienta R4000 analyzer at a 3 K sample temperature. The Sb, Bi and Cr concentrations in the films were determined by using inductively coupled plasma atomic emission spectroscopy (ICP-AES). The structural characteristics of BST films were investigated by using TEM (FEI Tecnai F20; acceleration voltage, 200 kV) and XRD (Rigaku TTR-Ⅲ, Japan).

Transport measurement.—The Bi_2Te_3, BST and CBST thin films were mechanically scratched into six-terminal Hall bar configurations by a sharp metal tip; then, aluminum wires were glued to each terminal with silver epoxy to form ohmic contacts. The R_{xx} and R_{xy} data were symmetrized and antisymmetrized, respectively, to account for the misalignment of electrodes. The transport measurements were carried out using a 9 T Physical Properties Measurement System (PPMS, Quantum Design) with a base temperature of 2 K.

References

[1] Hasan M Z and Kane C L 2010 *Rev. Mod. Phys.* **82** 3045
[2] Qi X L and Zhang S C 2010 *Phys. Today* **63** 33
[3] Fan Y B et al 2014 *Nat. Mater.* **13** 699
[4] Fan Y B et al 2016 *Nat. Nanotechnol.* **11** 352
[5] Yasuda K et al 2017 *Phys. Rev. Lett.* **119** 137204
[6] Han J H et al 2017 *Phys. Rev. Lett.* **119** 077702
[7] Dc M et al 2018 *Nat. Mater.* **17** 800
[8] He Q L et al 2018 *Phys. Rev. Lett.* **121** 096802
[9] Wang Y et al 2017 *Nat. Commun.* **8** 1364
[10] He Q L et al 2017 *Nat. Mater.* **16** 94
[11] Mogi M et al 2017 *Nat. Mater.* **16** 516
[12] Šmejkal L et al 2018 *Nat. Phys.* **14** 242
[13] Chen Y L et al 2009 *Science* **325** 178
[14] Xia Y et al 2009 *Nat. Phys.* **5** 398
[15] Checkelsky J G et al 2011 *Phys. Rev. Lett.* **106** 196801
[16] Peng H et al 2010 *Nat. Mater.* **9** 225
[17] Wang Z H, Yang L, Li X J, Zhao X T, Wang H L, Zhang Z D and Gao X P 2014 *Nano Lett.* **14** 6510
[18] Chen X, Ma X C, He K, Jia J F and Xue Q K 2011 *Adv. Mater.* **23** 1162
[19] Taskin A A, Sasaki S, Segawa K and Ando Y 2012 *Adv. Mater.* **24** 5581
[20] Chang C Z, Zhang J S, Feng X, Shen J, Zhang Z C, Guo M H, Li K, Ou Y B, Wei P, Wang L L, Ji Z Q, Feng Y, Ji S H, Chen X, Jia J F, Dai X, Fang Z, Zhang S C, He K, Wang Y Y, Lu L, Ma X C and Xue Q K 2013 *Science* **340** 167
[21] Wang W J, Gao K H and Li Z Q 2016 *Sci. Rep.* **6** 25291
[22] Sapkota Y R and Mazumdar D 2018 *J. Appl. Phys.* **124** 105306
[23] Wang J, DaSilva A M, Chang C Z, He K, Jain J K, Samarth N, Ma X C, Xue Q K and Chan M H W 2011 *Phys. Rev. B* **83** 245438
[24] He X Y, Guan T, Wang X X, Feng B J, Cheng P, Chen L, Li Y Q and Wu K H 2012 *Appl. Phys. Lett.* **101** 123111
[25] Checkelsky J G, Yoshimi R, Tsukazaki A, Takahashi K S and Tokura Y 2014 *Nat. Phys.* **10** 731
[26] Kong D S, Chen Y L, Cha J J, Zhang Q F, Analytis J G, Lai K J, Liu Z K, Hong S S, Koski K J and Mo S K 2011 *Nat. Nanotechnol.* **6** 705
[27] Shimizu S, Yoshimi R, Hatano T, Takahashi K S, Tsukazaki A, Kawasaki M, Iwasa Y and Tokura Y 2012 *Phys. Rev. B* **86** 045319
[28] Yoshimi R, Tsukazaki A, Kozuka Y, Falson J, Takahashi K S, Checkelsky J G, Nagaosa N, Kawasaki M and Tokura Y 2015 *Nat. Commun.* **6** 6627
[29] Lee J S, Richardella A, Hickey D R, Mkhoyan K A and Samarth N 2015 *Phys. Rev. B* **92** 155312
[30] Tian J F, Chang C Z, Cao H L, He K, Ma X C, Xue Q K and Chen Y P 2015 *Sci. Rep.* **4** 4859
[31] Islam S, Bhattacharyya S, Kandala A, Richardella A, Samarth N and Ghosh A 2017 *Appl. Phys. Lett.* **111** 062107
[32] Cha J J, Williams J R, Kong D, Meister S, Peng H, Bestwick A J, Gallagher P, Goldhaber G D and Cui Y 2010 *Nano Lett.* **10** 1076
[33] Hor Y S, Roushan P, Beidenkopf H, Seo J, Qu D, Checkelsky J G, Wray L A, Hsieh D, Xia Y, Xu S Y, Qian D, Hasan M Z, Ong N P, Yazdani A and Cava R J 2010 *Phys. Rev. B* **81** 195203
[34] Checkelsky J G, Ye J T, Onose Y, Iwasa Y and Tokura Y 2012 *Nat. Phys.* **8** 729
[35] Li H, Song Y R, Yao M Y, Yang F, Miao L, Zhu F F, Liu C H, Gao C L, Qian D, Yao X, Jia J F, Shi Y J and Wu D 2012 *Appl. Phys. Lett.* **101** 072406
[36] Li B, Fan Q Y, Ji F H, Liu Z, Pan H and Qiao S 2013 *Phys. Lett. A* **377** 1925
[37] Chang C Z, Zhang J S, Liu M H, Zhang Z C, Feng X, Li K, Wang L L, Chen X, Dai X and Fang Z 2013 *Adv. Mater.* **25** 1065
[38] Nagaosa N, Sinova J, Onoda S, MacDonald A H and Ong N P 2010 *Rev. Mod. Phys.* **82** 1539
[39] Kou X F, Lang M R, Fan Y B, Jiang Y, Nie T X, Zhang J M, Jiang W J, Wang Y, Yao Y G, He L and Wang K L 2013 *ACS Nano* **7** 9205
[40] Chang C Z, Zhao W, Kim D Y, Zhang H J, Assaf B A, Heiman D, Zhang S C, Liu C X, Chan M H W and Moodera J S 2015 *Nat. Mater.* **14** 473
[41] Kandala A, Richardella A, Kempinger S, Liu C X and Samarth N 2015 *Nat. Commun.* **6** 7434

Supplementary Materials: Electrically Tunable Wafer-Sized Three-Dimensional Topological Insulator Thin Films Grown by Magnetron Sputtering

Qixun Guo(郭奇勋)[1], Yu Wu(吴宇)[1], Longxiang Xu(徐龙翔)[1], Yan Gong(龚演)[2], Yunbo Ou(欧云波)[2], Yang Liu(刘洋)[1], Leilei Li(李磊磊)[1], Yu Yan(岩雨)[3]**, Gang Han(韩刚)[4], Dongwei Wang(王东伟)[5], Lihua Wang(王立华)[6], Shibing Long(龙世兵)[7], Bowei Zhang(张博威)[8], Xun Cao(曹迅)[8], Shanwu Yang(杨善武)[4], Xuemin Wang(王学敏)[4], Yizhong Huang(黄一中)[8], Tao Liu(刘涛)[9], Guanghua Yu(于广华)[1], Ke He(何珂)[2]**, Jiao Teng(滕蛟)[1]**

[1]Department of Material Physics and Chemistry, University of Science and Technology Beijing, Beijing 100083, P. R. China
[2]State Key Laboratory of Low-Dimensional Quantum Physics, Tsinghua University, Beijing 100084, P. R. China
[3]Corrosion and Protection Center, Key Laboratory for Environmental Fracture (MOE), Institute of Advanced Materials and Technology, University of Science and Technology Beijing, Beijing 100083, P. R. China
[4]Collaborative Innovation Center of Advanced Steel Technology, University of Science and Technology Beijing, Beijing 100083, P. R. China
[5]CAS Key Laboratory of Standardization and Measurement for Nanotechnology, National Center for Nanoscience and Technology, Beijing 100190, P. R. China
[6]Institute of Microstructure and Property of Advanced Materials, Beijing Key Lab of Microstructure and Property of Advanced Materials, Beijing University of Technology, Beijing, 100124, P. R. China
[7]School of Microelectronics, University of Science and Technology of China, Hefei, 230026, P. R. China
[8]School of Materials Science and Engineering, Nanyang Technological University, 50 Nanyang Avenue, 639798, Singapore
[9]Department of Physics, The Ohio State University, Columbus, Ohio 43210, USA

Table of contents:

Figure S1. Additional structural characterizations on Bi_2Te_3 thin films
Figure S2. Temperature dependence of the sheet resistance R_{xx} of Bi_2Te_3 thin films
Figure S3. Hall measurements of a 10 nm Bi_2Te_3 thin film
Figure S4. Hall bar structure for transport measurement
Figure S5. Data symmetrization
Figure S6. Hall angle (R_{AH}/R_{xx}) as a function of back gate V_g of the CBST thin films
Figure S7. Gate-dependent magneto-transport measurements on $Cr_{0.24}(Bi_{0.33}Sb_{0.67})_{1.76}Te_3$ thin film.

Figure S1. Additional structural characterizations on Bi_2Te_3 thin films. (a) Atomic force microscopy (AFM) topographic image of a 10 nm Bi_2Te_3 thin film grown by magnetron sputtering. (b), (c) Height profile along the solid red and green line marked in (a), respectively. AFM measurements reveal steps with a height of nearly 1 nm, corresponding to a quintuple layer (QL). The presence of multiple steps in Bi_2Te_3 thin films implies a layer-by-layer growth process during the magnetron co-sputtering, which is similar to MBE and other methods.[1,2]

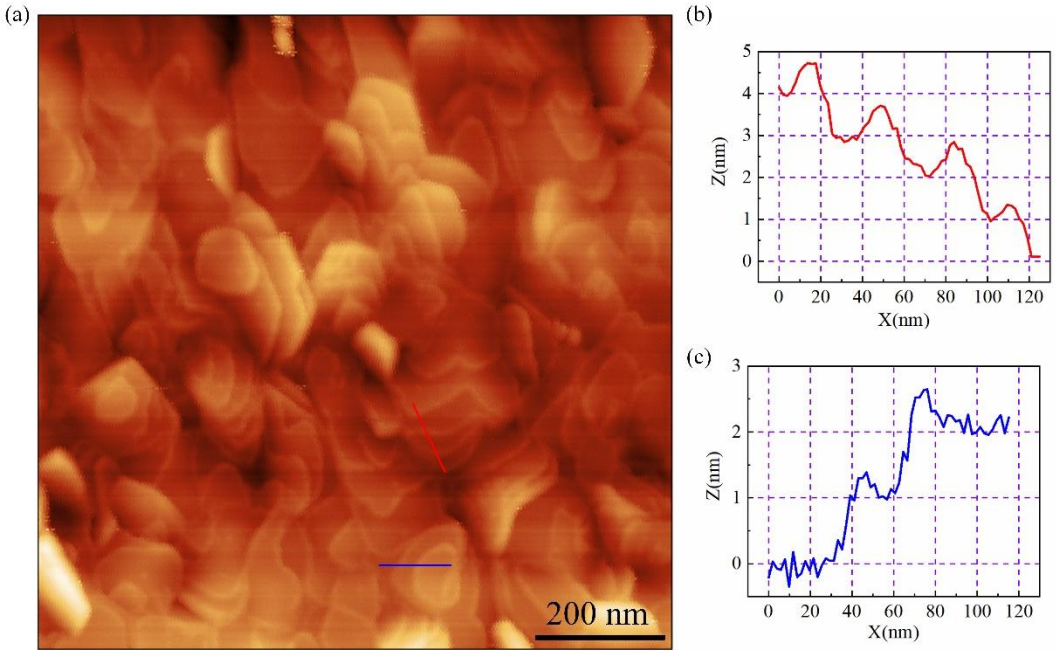

Figure S2. Temperature dependence of the sheet resistance R_{xx} of Bi_2Te_3 thin films. Sheet resistance R_{xx} vs temperature of a 10 nm Bi_2Te_3 thin films from 300 K to 10 K (a), from 10 K to 2 K (b). In panel (b), the straight line is linear fit of R_{xx} to ln$T$.

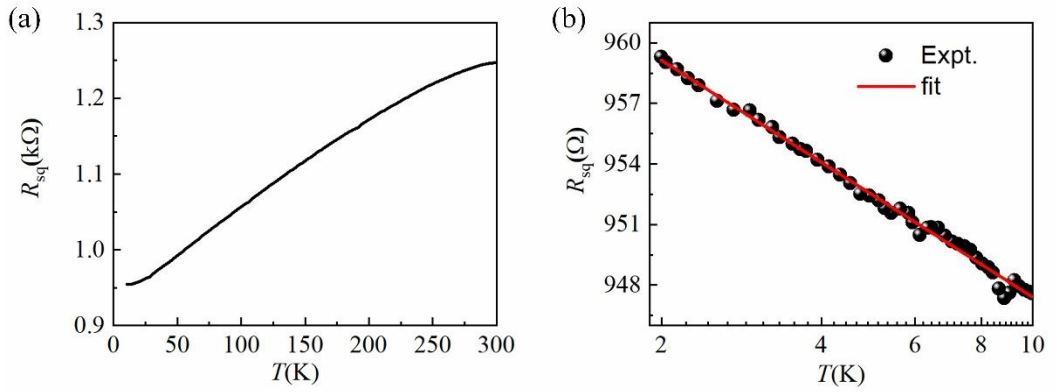

In the 10 nm sputtered Bi_2Te_3 thin film, with decreasing temperature, R_{xx} displays metallic behavior at high temperature region (from 300 K to 10 K) and becomes weakly insulating behavior at low temperature region (from 10 K to 2 K). The R_{xx} increases logarithmically with T at low temperature region, possibly due to the coexistence and competition of weak antilocalization and electron-electron interaction.[3-5]

Figure S3. Hall measurements of a 10 nm Bi_2Te_3 thin film. (a) Hall resistance as a function of the magnetic field at different temperatures. The negative slopes of Hall traces verify that the electrons are the major carriers. (b) The carrier density and mobility are shown as a function of temperature. Both the carrier density and mobility show little dependence on temperature, indicating that our sample is in the metallic region.

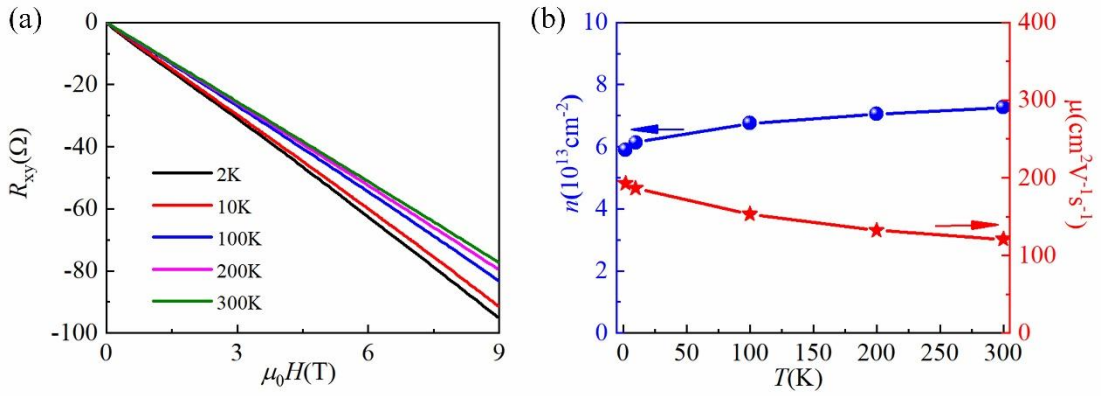

Figure S4. Hall bar structure for transport measurement. (a) schematic diagram of the mm-sized Hall bar structure, where the heavily doped Si substrate (with 300 nm SiO_2 overlayer) is used as a backgate to tune the Fermi level of the bottom surface. (b) Optical image of a Hall bar device mechanically scratched by a sharp metal tip for subsequent transport measurement.

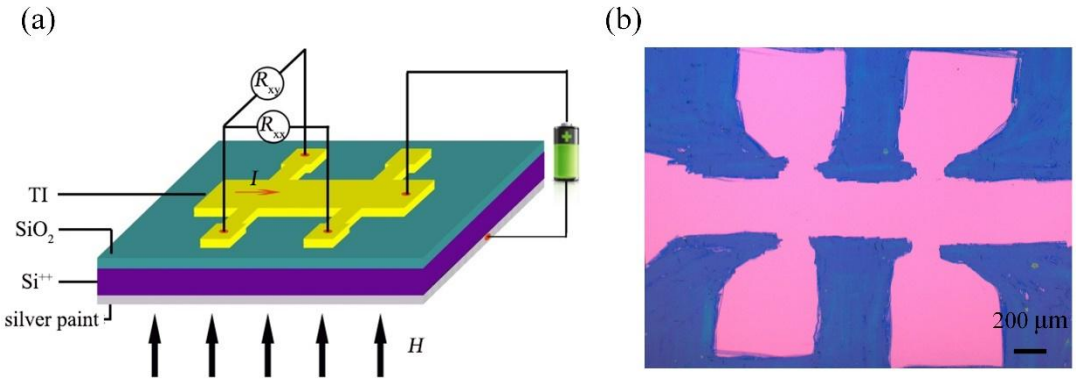

Figure S5. Data symmetrization. (a)-(b) The raw data of R_{xx} and R_{xy} of a CBST sample. Since the Hall bars are manually scratched, a mixing of the signals between R_{xx} and R_{xy} is inevitable for the misalignment of electrodes. (c)-(d) The symmetrized data of R_{xx} and R_{xy} in (a) and (b), respectively. Here, the symmetrized R_{xx} and R_{xy} are obtained by following two equations: $R_{xx}^{sym}(H)=[R_{xx}^{raw}(H)+R_{xx}^{raw}(-H)]/2$, $R_{xy}^{sym}(H)=[R_{xy}^{raw}(H)-R_{xy}^{raw}(-H)]/2$.

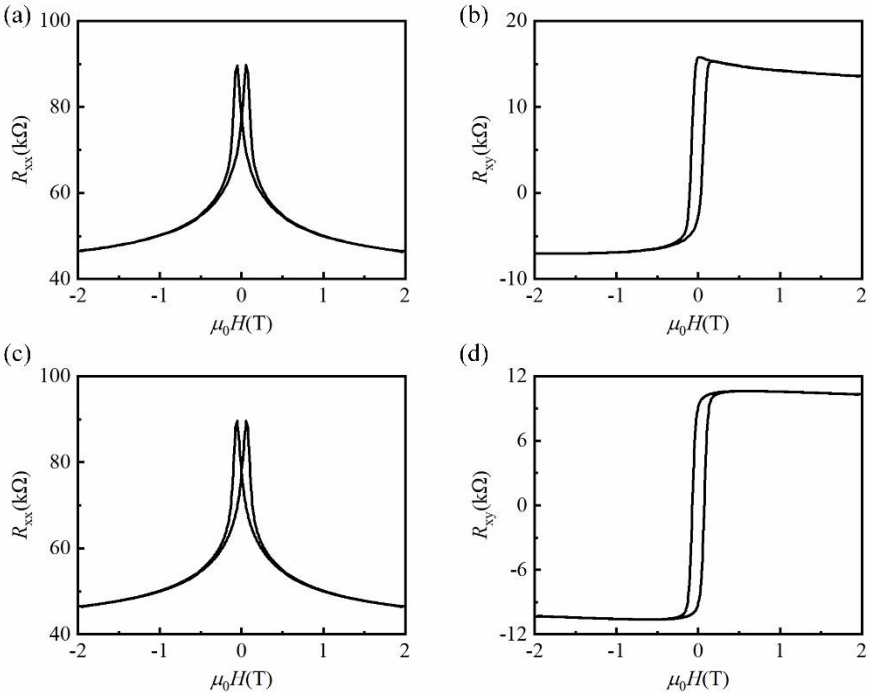

Figure S6. Hall angle (R_{AH}/R_{xx}) as a function of back gate V_g of the CBST thin films. The maximum value of Hall angle of this sample reaches 20% at T=2 K.

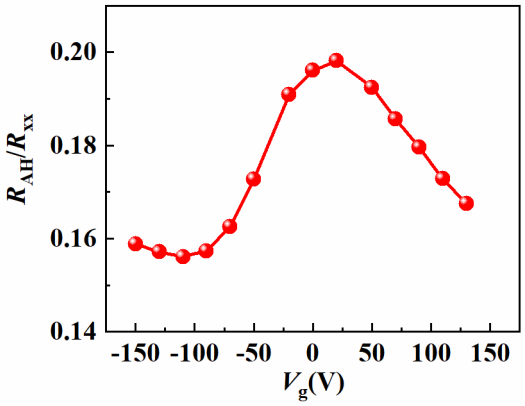

Figure S7. Gate-dependent magneto-transport measurements on $Cr_{0.24}(Bi_{0.33}Sb_{0.67})_{1.76}Te_3$ thin film. (a) Hall resistance R_{xy} and (b) longitudinal sheet resistance R_{xx} vs $\mu_0 H$ at different gate voltages at a temperature of 2 K. Dependence of Hall coefficient R_H (c) and zero field longitudinal sheet resistance R_{xx} (d) on the back-gate voltage. The carrier type is tuned from *p*- to *n*-type with the gate voltage increased from -150 to +150 V.

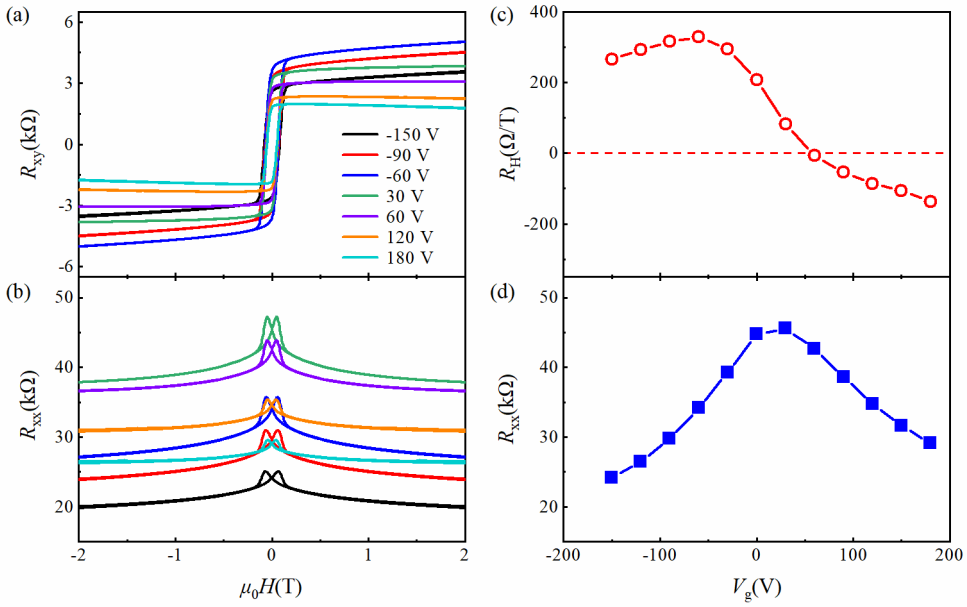

References

[1] Li Y Y, Wang G, Zhu X G, Liu M H, Ye C, Chen X, Wang Y Y, He K, Wang L L and Ma X C 2010 *Adv. Mater.* **22** 4002

[2] Kong D S, Randel J C, Peng H L, Cha J J, Meister S, Lai K J, Chen Y L, Shen Z X, Manoharan H C and Cui Y 2010 *Nano Lett.* **10** 329

[3] Wang J, DaSilva A M, Chang C Z, He K, Jain J K, Samarth N, Ma X C, Xue Q K and Chan M H W 2011 *Phys. Rev. B* **83** 245438

[4] Chen J, He X Y, Wu K H, Ji Z Q, Lu L, Shi J R, Smet J H and Li Y Q 2011 *Phys. Rev. B* **83** 241304

[5] Zhao Y F, Chang C Z, Jiang Y, DaSilva A, Sun Y, Wang H C, Xing Y, Wang Y, He K, Ma X C, Xue Q K and Wang J 2013 *Sci. Rep.* **3** 3060